Launcher Study for KSTAR 5GHz LHCD System*

[a)]Y. S. Bae, [a)]M. H. Cho, [a)]W. Namkung, [b)]S. Bernabei, [b)]R. Ellis, [b)]J. Wilson, [b)]J. Hosea, and [b)]H. Park
[a)]Physics Department, POSTECH, Pohang 790-784, Korea
[b)]Princeton Plasma Physics Laboratory, Princeton, NJ08543, USA

Abstract

A 5-GHz Lower Hybrid Current Drive (LHCD) system with 2-MW is under development for the steady-state operations of the KSTAR. The present design of fully active waveguide launcher gives very good spectral directivity of more than 90% for the phase shift of 90 degrees and a wider $N_{\parallel}$ range of 1.4 to 3.6 with a width $\Delta N_{\parallel}$ = 0.54. For the steady-state operations of the KSTAR, a Glidcop/SS sandwich grill is proposed with consideration of heat and disruption loads. A PAM (Passive-Active Multi-junction)-type launcher is also studied for the possibility of using for the KSTAR. The PAM-type launcher provided good coupling properties even at lower edge densities in FTU 8 GHz PAM launcher tests. However, it gives a lower current drive efficiency compared with the conventional grill because of reduced directivities. The Passive/Active grill has 30 % reduced directivity than the Fully Active grill from the characteristic studies on the directivity and coupling. On the other hand, it gives a good coupling property with weakly dependence on the phase shift between adjacent waveguides

1. Introduction

The recent interests for the LHCD system are mainly to control and to shape the plasma current profiles rather than the plasma heating [1]. The off-axis current driven by the LH waves can create broad or even hollow current profiles required in the 'advanced tokamak' scenario for ITER by introducing a negative shear [2]. Therefore, the LH system is expected to provide a major contribution to the advanced tokamak experiments in the steady-state KSTAR operations (300 s). The KSTAR 5-GHz, 2-MW CW LHCD system is under development. The RF frequency of LH wave is chosen as 5 GHz for the KSTAR, which is the same as the ITER LH frequency. For 5 GHz RF source, an order for proto-type of 5-GHz, 500-kW CW klystron is placed to Toshiba Electron Tubes & Devices (TETD) Co., and it is under fabrication.

Phased waveguide arrays are generally being used for launching LH waves in tokamak. The concept of the conventional 'grill' [3] – an array of independent waveguides – is used to design the KSTAR LH launcher. In recent years, the basic design on the 5-GHz LH launcher with fully active waveguide channels has been carried out in collaboration with PPPL [4, 5]. The design has many features the same as in the C-MOD LHCD system, which will serve to test these features for relatively short pulses of 5 s.

The near steady-state of the KSTAR operation, however, requires somewhat new challenges of heat removal in the grill and of compact water-loads absorbing the reflected RF power. It also introduces that the ITER-relevant launcher based on the PAM (Passive Active Multi-junction) concept could be an alternative candidate for the KSTAR LH launcher because the PAM launcher was successfully validated in FTU [6]. The test of a PAM launcher on FTU shows the first step toward the LHCD launcher for ITER. In this paper, the present design of 5 GHz KSTAR LH launcher is described in sections 2 and 3. The PAM launcher test on FTU is introduced in section 4. Also the PAM concept on the KSTAR LH launcher is compared with the fully active launcher for the power directivity and the coupling followed by conclusions.

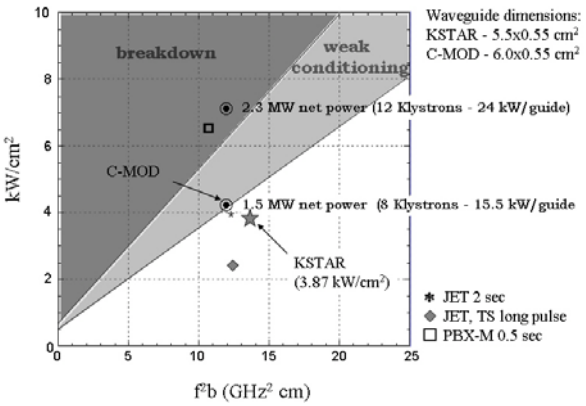

Fig. 1. Power flux density in C-MOD and KSTAR grill [5].

2. 5 GHz KSTAR LH launcher

2.1 Power spectrum and coupling properties

The present design of 5 GHz KSTAR LH launcher has a very good spectral controllability by phasing of each waveguide column in the grill. The grill is composed of fully 32 active waveguide columns by 4 rows. Each waveguide width and height is 5.5 mm and 55.0 mm, respectively, and it is separated by a 1.5-mm thick septum. The waveguide size in the grill is compromised for the power flux density in the grill below a weakly breakdown conditioning regime as shown in Fig. 1 as well as for higher fundamental peak

* Work supported by KSTAR project, NFRC

$N_{\parallel}$ (see Eq. (1)) than the accessible $N_{\parallel}$ given by the Golant condition (see Eq. (2)).

$$N_{\parallel n} = \frac{\Delta\phi}{kp} + n\frac{\pi}{kp} \tag{1}$$

$$N_{\parallel,\,acc} = \frac{\omega_{pe}}{\omega_{ce}} + \left[1 + \frac{\omega_{pe}^2}{\omega_{ce}^2} - \frac{\omega_{pi}^2}{\omega^2}\right]^{1/2} = 3.21\frac{\sqrt{n_e}}{B_T} + \left[1 + \frac{10.33}{B_T^2} n_e \left(1 - 0.427\, A\frac{B_T^2}{f_{LH}^2}\right)\right]^{1/2} \tag{2}$$

Where, k is the vacuum wave-number, $\Delta\phi$ is the phase shift between adjacent waveguides, p is the geometric periodicity of waveguides, and n is an integer mode number. The positions of the fundamental peak $N_{\parallel 0}$ of the radiated spectrum is 2.13 for the KSTAR LH grill with p = 7 mm, $\Delta\phi = \pi/2$. Fig. 2 shows the radiated power spectra and the integrated coupling power efficiency over $N_{\parallel}$ for various phase shifts using the Steven's code [7]. The accessible $N_{\parallel}$ = 2.0 is given for f_{LH} = 5 GHz, B_T = 3.5 T, A is the atomic mass number of hydrogen of 1, and n_e = 1x10^{20} m^{-3}, $N_{\parallel acc}$ = 2.0.

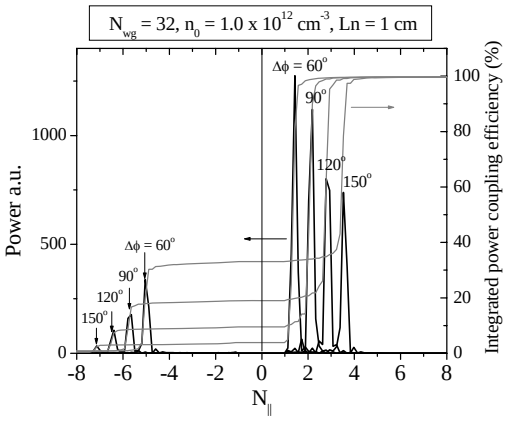

Fig. 2. Radiated power spectrum and integrated power coupling efficiency over $N_{\parallel}$ are for their phase shifts of 60°, 90°, 120°, and 150° with the edge density, n_0 = 1x10^{12} cm^{-3} and the density gradient, $\nabla n = n_0/L_n$ = 1x10^{13} cm^{-3}.

The power directivity, D_p and the $N_{\parallel}$-weighted directivity, D_{cd} which is defined with respect to the current drive efficiency, are given by

$$D_p = \int_1^{\infty}\frac{dP}{dN_{\parallel}}dN_{\parallel} \Big/ \int_{-\infty}^{\infty}\frac{dP}{dN_{\parallel}}dN_{\parallel}$$
$$D_{cd} = (1-R)N_{\parallel peak}^2\left(\int_1^{\infty}\frac{1}{N_{\parallel}^2}\frac{dP}{dN_{\parallel}}dN_{\parallel} - \int_{-\infty}^{-1}\frac{1}{N_{\parallel}^2}\frac{dP}{dN_{\parallel}}dN_{\parallel}\right) \tag{3}$$

respectively. From the vertical axis of right hand side in Fig. 2, the power directivities are easily obtained as 96 %, 91 %, 81 %, and 67 % for each phase shift of 60°, 90°, 120°, and 150°. But, the definition of D_{cd} gives $N_{\parallel}$-weighted directivities of 93 %, 89 %, 72 %, and 45 %. Fig. 3 shows the directivities as a function of the grill edge plasma density. The maximum value of $N_{\parallel}$-weighted directivities corresponds to the minimum reflection at the same edge density.

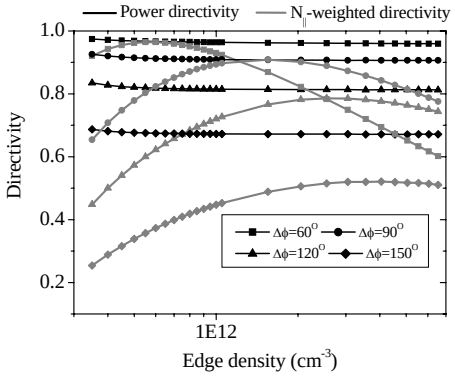

Fig. 3. Two different directivities as a function of grill edge plasma density.

The optimum coupling edge density at the grill is calculated using the linear coupling theory in two regimes: a) the "cutoff regime" at a lower density, b) the "WKB regime" at a moderate density without taking into consideration of high density effect where $\boldsymbol{E} \times \boldsymbol{B}$ current cannot be neglected [8]. The density gradient is a key parameter in the cutoff regime at low edge density, and the edge density is a key parameter in the "WKB regime" at moderate density. For the "WKB" regime, the optimum edge density ratio to the cutoff density is theoretically given by [7]

$$\frac{n_0}{n_c} = N_{\parallel}^2\left(1 - \left(\frac{\pi}{k_0 h}\right)^2\right) + \left(\frac{\pi}{k_0 h}\right)^2 \tag{4}$$

Where, n_0 is the edge density at grill, n_c is the cutoff density where the plasma frequency is the same as the LH wave frequency (n_c = 3 x 10^{11} cm^{-3} for 5 GHz), and h is the waveguide height. For KSTAR, n_0/n_c = 3.54 for $\Delta\phi = \pi/2$ (peak $N_{\parallel}$ = 2.15). Fig. 4 shows the results by the Steven's code on the coupling effects of the fully active grill for the KSTAR on low edge density and moderate density regimes using step and linear density ramping in front of the grill.

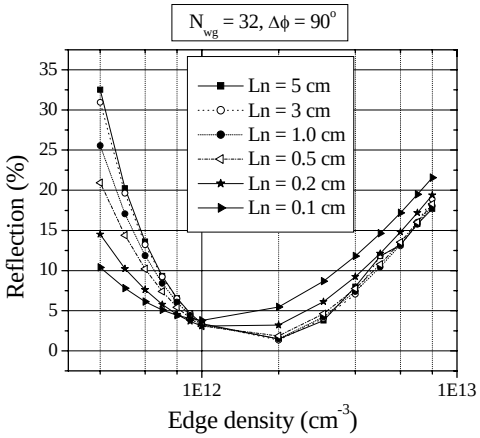

Fig. 4. The reflection from the grill edge as a function of edge density for various scale lengths of the density gradient.

It shows the best coupling edge density is about 3.3 n_c ~ 1 x 10^{12} cm^{-3} for the scale length less than 0.2 cm. One may note that the coupling has the less density gradient dependency for the edge density higher than 8x10^{11} cm^{-3}. The best coupling with the minimum reflection, which is less than 2 %, is obtained with the edge density around 2x10^{12} cm^{-3}.

2.2 Waveguide channel design

The KSTAR LH launcher is composed of 64 waveguide channels, 32 channels each for the upper and lower modules, patterned on the metal plate. The grill is attached to the end of waveguide channels. The channels are stacked with bolts through the metal plates. The waveguide pattern in each channel is shown in Fig. 5.

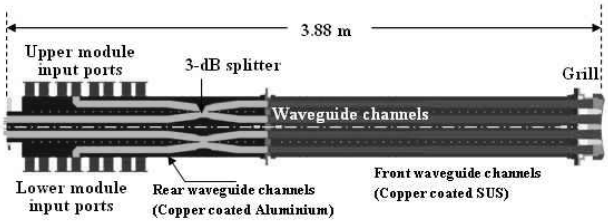

Fig. 5. The cross section drawing of waveguide channel.

The key pattern is 3-dB power splitter for evenly power splitting into the vertical output waveguides. The optimized design of the 3-dB power splitter is obtained by introducing a capacitive button at the center of the 3-dB power splitter. It is just an extruding metal cylinder with a height of 1.3 mm. Fig. 6 shows the test module of the 3-dB power splitter with a capacitive button and HFSS simulation results. From the low power test of the test module, the same output power of -3.43 dB at each output waveguide is obtained, and the return loss (S11) and the isolation to the matched waveguide (S31) are all less than -30 dB.

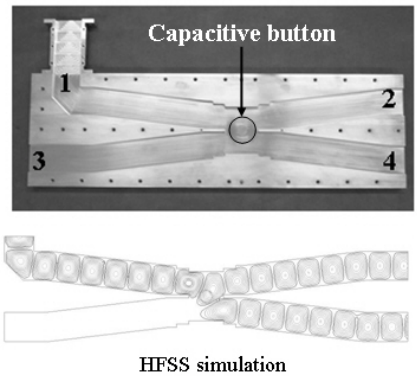

Fig. 6. (Upper) A test module of 3-dB power splitter and (lower) the electric field contour plot in HFSS simulation.

3. Steady-state design issues for the KSTAR LH launcher

The present design of the KSTAR LH launcher has many features as the C-MOD LH launcher. However, the long pulse (300 s) operation of the KSTAR requires some new design considerations for the KSTAR LH launcher. The requirements and challenges for the new launcher features are; better heat removal from the grill nose, shielding of the microwave windows from direct line of sight to the plasma, and compact water loads for capturing and absorbing power reflected from the grill edge plasma. The heat removal from the grill nose is the major critical issue for the steady-state operation. Two possible solutions for KSTAR LH launcher cooling could be as follows.

1. Incorporate Frascati ITER PAM grill type; it is good for the good cooling but reduces active guides by half and reduces the directivity of radiated power spectrum.
2. Design the cooling into the present stacked metal plate of the KSTAR launcher design; it keeps the optimum spectral control but the 1.5 mm Stainless Steel septum could not provide the heat conductivity.

For the second solution, the material must be changed to Glidcop or CuCrZr or cooling tubes imbedded into septum. A proper design of Glidcop/SS sandwiched grill, that is, a stacked construction with Glidcop septum and water cooled Stainless Steel insert as seen in Fig. 7, is obtained using the ANSYS program [9] in collaboration with PPPL [5]. ANSYS finite element model of Glidcop/SS sandwiched grill is shown in Fig. 7, using SOLID90 thermal elements and SURF152 elements to specify radiation and heat convection boundary conditions, was constructed for the configurations to be studied.

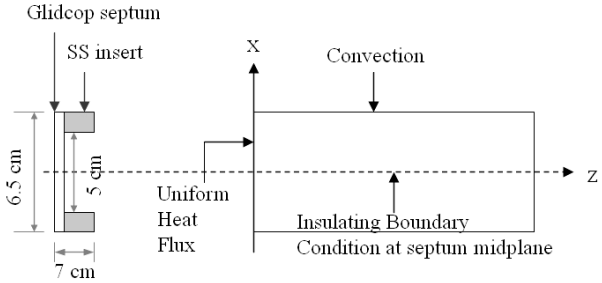

Fig. 7. Schematic of 3-dimensional ANSYS finite element model for the stacked construction with Glidcop septum and cooled SS insert.

In this model, the x, y, and z coordinates correspond to the vertical, toroidal, and outward radial directions. For the simplicity, the only half waveguide is used using the insulating boundary condition on septum mid-plane. The uniform heat flux from the plasma is assumed 100 W/cm^2. The convection film coefficient for the top of grill water cooled within 5 mm from front edge is set to 1.6 $W/cm^2 \cdot K$ with the water coolant bulk temperature of 20°C. The thermal conductivity for the Glidcop septum and SS insert are given by the function of the temperature

$$k_{Glidcop} = 3.65 - 0.00052\,T \ [\mathrm{W/cm^2 \cdot K}]$$
$$k_{SS} = 0.163 + 0.000147\,T \ [\mathrm{W/cm^2 \cdot K}] \quad (5)$$

Fig. 8 shows the ANSYS analysis result. The maximum temperature of 580°C is seen in the front edge of SS insert and therefore this design would be the adequate performance for the steady state operation on the KSTAR.

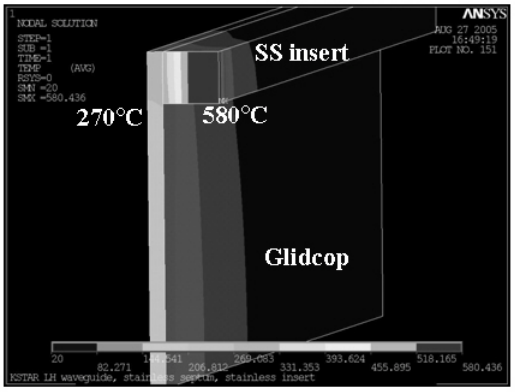

Fig. 8. Temperature distribution results from ANSYS simulation.

4. Characteristics of PAM launcher and Basic Studies on Passive/Active grill for KSTAR

In this section, the concept of PAM (Passive-Active Multi-junction) launcher and FTU PAM launcher test results are introduced. Also, the basic characteristics of Passive-Active grill with the passive waveguide 90° phased are compared with those of the fully active grill.

The necessity of the passive waveguide is originated from minimizing the surface wave component of the radiated power because surface waves give rise to undesirable non-linear interactions [10-13]. Surface wave can be minimized by employing multiple waveguide arrays as well as by driving the outside guides at a reduced power [14]. It was observed that the reduction in the width of the resonance cone and in the amplitude of the surface wave component by a factor of ~ 3 when the passive waveguides (tuners or dummy guides) are added in each side of twin guide array [15].

The detailed results of LHCD and coupling experiments with the ITER-like PAM launcher at 8 GHz at FTU is found in reference 6. Fig. 9 shows the ITER-like PAM launcher used at FTU. The maximum achieved value of the routine power density was 80 MW/m^2 that would be only 52 MW/m^2 by scaling with the frequency. This is at least 1.4 times larger than the ITER request of 33 MW/m^2 required to the ITER grill in order to couple 20 MW to the plasma. Also, they obtained very good coupling throughout the SOL plasma, provided the antenna is properly conditioned to avoid gas release from the internal waveguide walls. The average reflection coefficient ρ_c is $\approx$ 1.3%, and never exceeded 2.5%, even with almost evanescent plasmas in front of the grill, as when this was fully retracted inside the port (up to 3 mm) to simulate the ITER operation, and the density at its mouth is equal or even lower than the cut-off value. But, on the current drive (CD) efficiency, PAM CD is reduced. But authors in Ref. 6 conclude it is not degraded with respect to a conventional grill launching a similar $N_{||}$ spectrum, taking into account the lower power directivity.

The basic study on directivity and coupling characteristics of Passive-Active grill and Fully Active grill are carried out using the Steven's code also. For the Passive/Active grill, the simple model is shown in Fig. 10. It is assumed that every other passive waveguide is 90°-phased and 1-% field power crossed to the adjacent active waveguides in the calculation. Note that only first pass before the reflection back from the short plane of the passive waveguide and no multi-junction type are considered.

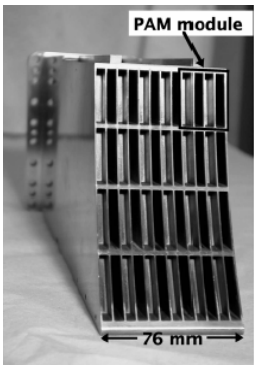

Fig. 9. FTU PAM launcher [6].

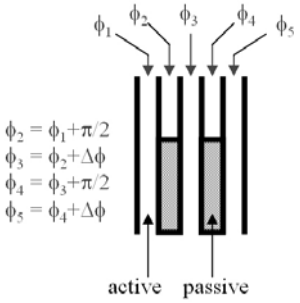

Fig. 10. Simple Passive-Active grill structure

Fig. 11 shows the radiated power spectrum from the fully active grill and the simple passive-active grill. The passive-active grill has many other peaks not having negligible power.

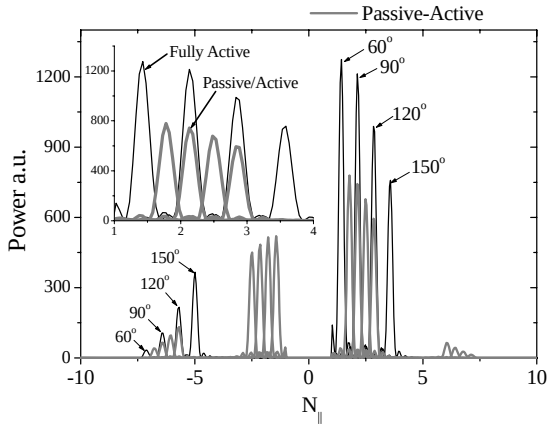

Fig. 11. Radiated power spectrum in passive-active grill and fully active grill for the phase shifts.

In Fig. 12, the directivity and the coupling are compared as a function of the phase shift between adjacent waveguides. The fully active grill gives much better directivity and wider N|| range compared with the

passive-active grill. The passive-active grill has the opposite N||-weighted directivity as the phase shift increases. But, for the coupling in the "WKB" regime of the edge density, the passive-active grill gives better coupling in a wide range of phase shifts as shown in Fig. 13.

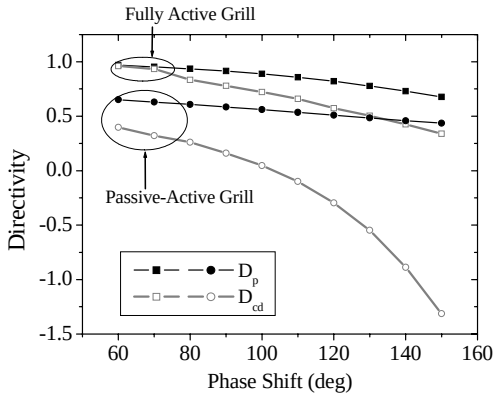

Fig. 12. Directivities as a function of phase shift for passive-active grill and fully active grill.

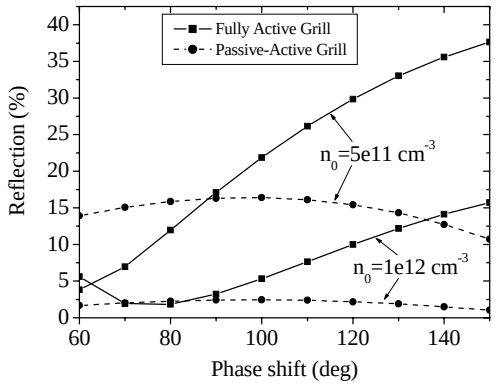

Fig. 13. Reflection as a function of phase shift for passive-active grill and fully active grill.

5. Conclusion

The fully active waveguides for the 5-GHz KSTAR LH launcher give a very good spectral directivity and a wider N||-range. The important issues for the steady-state KSTAR LH launcher are designing, analyzing, and high-power prototype of fully active grills that can sustain steady-state operations in the KSTAR. A Glidcop/SS sandwich would be best for heat and disruption loads although the detailed stress analysis is necessary in order to validate this design for the disruption load. The good metallic bonding between Glidcop and Stainless Steel could be possible if Ni-coated Glidcop would be brazed with Stainless steel. The further physical and mechanical engineering studies on this design will be continued in the near future.

The other issues are the proper placement of windows out-of-sight of plasma and the design of the compact water load for matched waveguide (arm 3) of the 3-dB power splitter and its prototype at low and high power levels.

The PAM launcher proves to have good coupling properties even at a lower edge density in FTU 8 GHz PAM launcher tests. However, it gives a lower current drive efficiency compared with the conventional grill because of reduced directivity. From the directivity and coupling studies for the Passive/Active grill and the Fully Active grill for the KSTAR, the Passive/Active grill has 30 % reduced directivity, but it gives a good coupling property with weakly dependence on the phase shift between adjacent waveguides. If lower $N_{||}$ proves to be optimum for the KSTAR, the PAM design could be an alternative for the KSTAR. In addition, it proves to be acceptable for the ITER.

REFERENCES

[1] X. Litaudon, R. Arslanbekov, G. T. Hoang et al., Plasma Phys. Controlled Fusion 38, 1603 (1996).
[2] J. Mailloux et al., Phys. Plasma 9, 2156 (2002).
[3] M. Brambilla, Nucl. Fusion 16, 47 (1976).
[4] Y. S. Bae, C. H. Paek, M. J. Rhee, W. Namkung, M. H. Cho, S. Bernabei, H. Park, Fusion Eng. Design 65, 569 (2003).
[5] J. Hosea, S. Bernabei, R. Ellis, and J. R. Wilson, "LHCD Steady-State Technology for KSTAR," US-Korea Workshop at GA, May 19-20 (2004).
[6] V. Pericoli Ridolfini et al., Nucl. Fusion 45, 1085 (2005).
[7] J. Stevens, M. Ono, R. Horton, J. R. Wilson, Nucl. Fusion 21, 1259 (1981).
[8] D. Moreau, C. Gormezano, G. Melin, T. K. Nguyen, in Radiation in Plasmas (Proc. Spring College Trieste, 1983), Vol. 1, World Scientific, Singapore (1984) 331.
[9] 3D Structural, Thermal, EM analysis software using Finite Element Method (FEM), Ansys Inc. , http://www.ansys.com/.
[10] G. J. Morales, Phys. Fluids 20, 1164 (1977)
[11] M. Porkolab, R. P. H. Chang, Rev. Mod. Phys. 50, 745 (1978).
[12] R. W. Motley, W. M. Hooke, G. Anania, Phys. Rev. Lett. 43, 1799 (1979).
[13] K. Matsuda, Y. Matsuda, G. E. Guest, General Atomic Report No. GA-A15351 (1979).
[14] V. Krapchev, A. Bers, Nucl. Fusion 18, 519 (1978).
[15] R. W. Motley, S. Bernabei, W. M. Hooke, F. J. Paoloni, Nucl. Fusion 20, 1207 (1980).